Brownian Processes in Human Motor Tasks: Behavioral Evidence of Velocity-level Planning

Federico Tessari [1], James Hermus [1], Rika Sugimoto-Dimitrova [1], Neville Hogan [1,2]

[1] Department of Mechanical Engineering, Massachusetts Institute of Technology, Cambridge, Massachusetts, USA

[2] Department of Brain and Cognitive Sciences, Massachusetts Institute of Technology, Cambridge, Massachusetts, USA

[*] Corresponding author

Email: ftessari@mit.edu

Abstract

Human postural control exhibits stochastic behavior resembling a random walk, which implies unbounded growth of position variance. Here we show that unbounded position variance is indeed observed in a common task, turning a crank. In postural tasks, intermittent control has been proposed to limit position variance. We further show that when position variance is unbounded, it displays a distinctive signature of underlying Brownian motion, a low-frequency power spectrum that declines at -20 dB/decade but exhibits flattening in bounded tasks. Remarkably, a descriptive model of a control system competent to account for all of these data must feature a forward-path velocity command corrupted by stationary noise. This provides independent behavioral support for the theory that the brain encodes motion commands in terms of velocity.

Introduction

During upright human posture, the center of pressure (CoP) of foot-floor interaction meanders within the foot-defined base of support in a manner resembling a random walk [1,2]. The archetypal random walk is a Brownian process [3] characterized by variance (second central moment) that grows linearly with time [4]. With unbounded variance, it is an unstable process and cannot be a competent description of CoP motion during stable upright posture. Intermittent feedback control has been proposed to limit the growth of variance [1,2,5,6].

However, the origin of the random walk and its implications for the control system architecture have not been established. Here we present experimental evidence of ubiquitous Brownian processes in several human motor tasks. We first show that unbounded linearly-growing variance, together with a linearly-decaying (-20 dB/dec) low-frequency power spectral density (PSD) – both defining features of a Brownian process – are indeed observed in human motor control, but only when the task permits unbounded variance. Conversely, in tasks in which variance must be bounded, e.g., maintaining static hand posture or standing balance, control mechanisms must eventually bound the process variance and flatten the low-frequency PSD. This is what we observed experimentally.

Brownian behavior can emerge from the control system in only three possible ways. We show that to account for all of the experimental evidence requires stationary noise corrupting forward-path velocity commands. Interestingly, these results provide independent behavioral support for the widely-debated hypothesis that the brain encodes motion commands in terms of velocity [7–12].

Results

Crank Turning

A crank-turning experiment was conducted with 10 subjects (Fig 1 left panel). Crank turning was selected since it is particularly common in human activities of daily living [13] but has the remarkable property of allowing unbounded motion despite the finite workspace of the human arm. Subjects were instructed to turn a crank at a constant speed in the clock-wise direction. Visual feedback of the rotational speed was provided. No explicit display of the angular position of the crank was provided, though normal proprioceptive feedback was available.

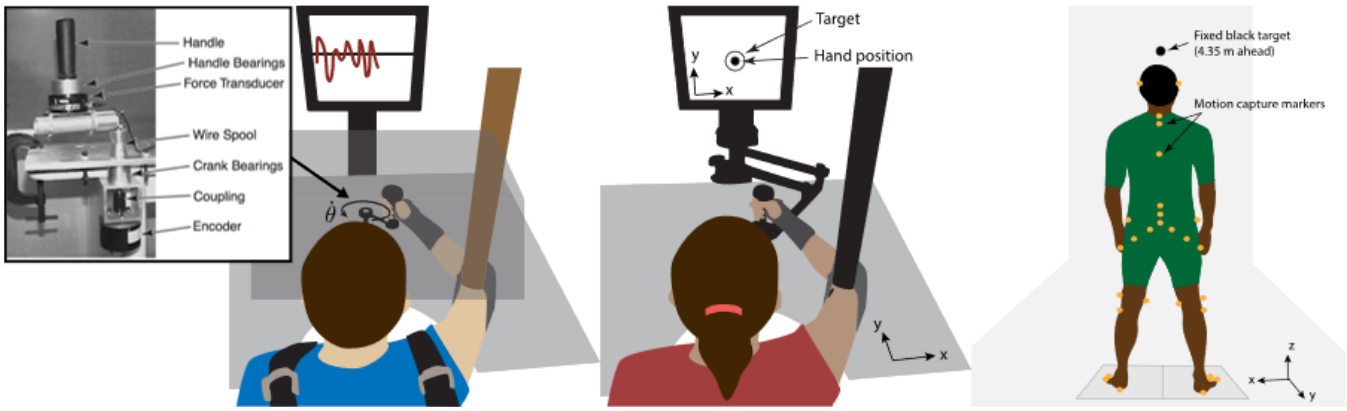

Fig 1. Experimental setups. (left) Crank turning: the crank displayed in the inset was used to provide a circular constraint. Vision of the arm and crank was occluded but the subject was provided with visual speed feedback. The wrist was braced, the upper arm was supported by a sling, and the shoulders were strapped to a chair. (center) Hand posture: the InMotion2 robot was used to measure hand position. Visual feedback of the hand position

was provided on the display. Vision of the arm and the robot was not occluded. The arm was supported by a sling. (right) Quiet standing [14]: subjects stood upright with their arms by their side, with their gaze fixed on a black target on a wall 4.35 m ahead. Motion capture markers were placed on their body. Further details of the three experiments are in the Material and Methods.

The experimental results for a representative subject performing the crank-turning task are presented in Fig 2. The three panels show: (i) the time trajectories of the crank angle over multiple crank rotations, (ii) the crank-angle variance, and (iii) the related PSD. The variance was computed across the ensemble (21 trials), while the PSD was computed for each trial and then averaged across trials.

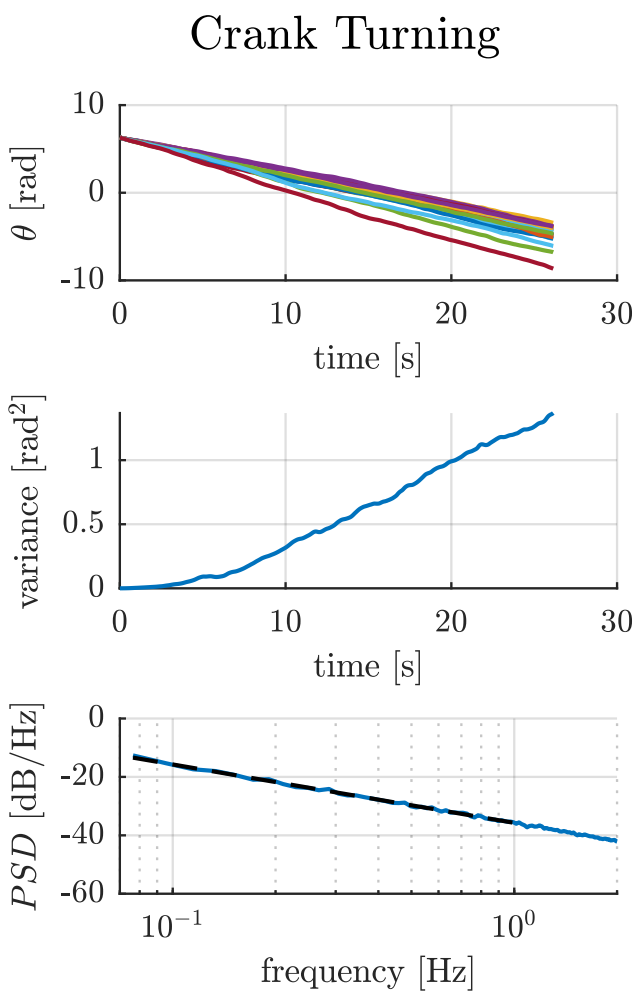

Fig 2. Crank turning experimental results for a representative subject. The top plot (2.1) shows the crank angular position trajectory over time for multiple trials. The central plot (2.2) presents the position variance computed across trials. The bottom plot (2.3) shows the average power spectral density of the angular position (solid blue line) compared to the best-fit line with a slope of -20.01 dB/dec (black dashed line).

The single-subject data in Fig 2 exhibit Brownian behavior – an unbounded, linearly-growing variance of crank angle with time ($R^2_{var} = 0.98$). In the frequency domain, we expected a -20 dB/dec slope in the PSD of the

crank angle, which we observed ($-20.01\ dB/dec$, $R^2_{PSD} = 0.997$), with 95% CI $[-20.35\ \ -19.67]$ dB/dec at the lowest frequencies (0.07-1 Hz).

The same behavior was observed across all subjects, with an average $R^2_{var} = 0.96 \pm 0.02$ for the variance slope, and an average PSD slope of -20.89 dB/dec ($R^2_{PSD} = 0.993 \pm 0.003$) with 95% CI of $[-21.40\ \ -20.36]$ dB/dec at low frequencies. The Supplementary Information contain R^2_{var} and R^2_{PSD} for the variance and PSD linear models and the 95% confidence intervals of the PSD slopes for all subjects.

Hand Posture

A postural task for the upper limb was devised (Fig 1 center panel) to assess whether the observed Brownian behavior is a peculiarity of tasks allowing unbounded motion. 10 subjects were asked to hold their hand in a fixed position for 4 minutes while visual feedback of hand position was provided. A sling supported the arm to minimize the gravitational load, while a robotic manipulandum with negligible friction was used to measure the planar (x,y) trajectory of the hand. 10 trials were performed.

The experimental results for a representative subject performing the hand-posture task are presented in Fig 3. The three panels show: (i) the time trajectories of hand position over the 10 trials, (ii) the hand-position variance, and (iii) the PSD of hand position. The x-coordinate of the hand position is presented; the y-coordinate (omitted for clarity) exhibited similar behavior.

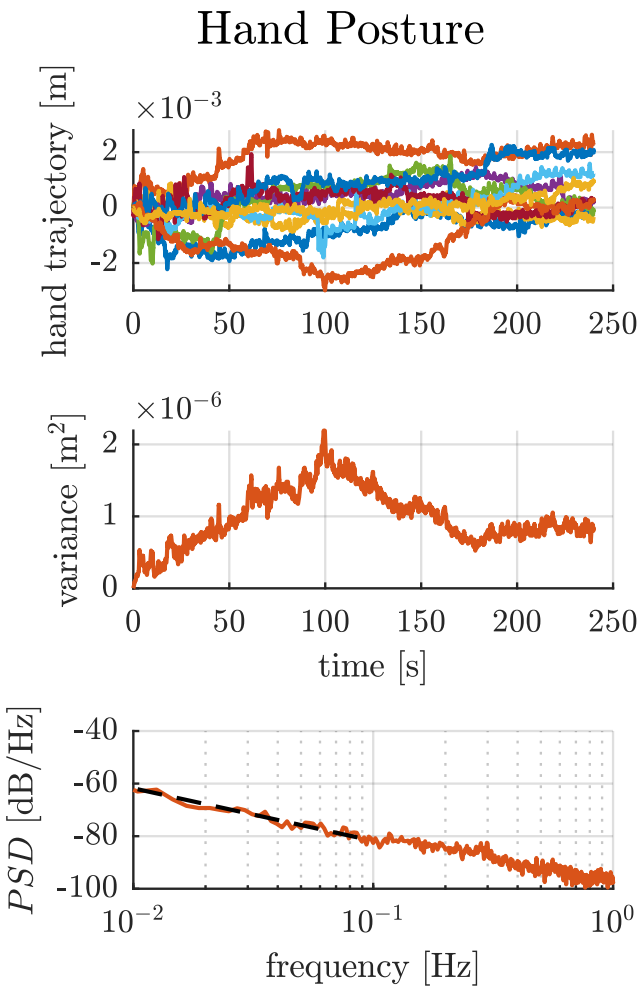

Fig 3. Hand posture experimental results of a representative subject. The top plot (3.1) shows the trajectories of the 'x' Cartesian coordinate of the hand over time for multiple trials. The central plot (3.2) presents the position variance computed across trials for the 'x' direction (red). The bottom plot (3.3) shows the average power spectral density of hand position in the 'x' direction (red) compared to the best-fit line with a slope of -18.46 dB/dec (black dashed line).

Once again, the single-subject data show that hand-position variance grew approximately linearly with time over the first minute in both the 'x' and 'y' directions ($R^2_{x_{var}} = 0.93,\ R^2_{y_{var}} = 0.95$), suggesting that the presence

of a Brownian process is an intrinsic feature of human neuromotor behavior. However, unlike in the crank-turning task, the hand-position variance reached a break point ($t_{bp_x} = 108\ s, t_{bp_y} = 61\ s$) after which the variance stopped its linear increase. In fact, linear regression of the variance computed over the whole time period showed a poor fit with $R^2_{x_{var}} = 0, R^2_{y_{var}} = 0.06$. The PSD displayed a -18.46 dB/dec slope ($R^2_{x_{PSD}} = 0.98$), with 95% CI $[-21.08\ -16.84]$ dB/dec in 'x' and a -21.39 dB/dec slope ($R^2_{y_{PSD}} = 0.93$) with 95% CI $[-23.16\ -19.61]$ dB/dec in 'y', over the low-frequency range (0.01-1 Hz).

In all 10 subjects, a consistent linearly-growing variance was observed, with an average $R^2_{var} = 0.85 \pm 0.1$. The breakpoint between linear growth and bounded variance varied across subjects, ranging from a few seconds (1-5 s) to minutes (100-135 s). Subjects' low-frequency PSDs presented good linear fitting ($R^2_{PSD} = 0.86 \pm 0.09$), with an average best-fitting slope of -16.69 dB/dec and an average 95% CI of $[-18.48\ -14.90]$ dB/dec in both directions. The minimum frequency for the linear fitting ranged from 0.01 Hz to 0.04 Hz across subjects. The flattening of the low-frequency PSD slope can be attributed to the boundedness of the process, and was reproduced in simulation (see the Descriptive Model below). The Supplementary Information report the variance and PSD coefficients of determination R^2_{var}, R^2_{PSD} and breakpoints, as well as the average PSD slope and related 95% confidence intervals for all 10 subjects.

Quiet Standing

An online data set was used to study behavior during natural upright posture [14]. This database contains observations of 49 subjects standing for 60 seconds at a time (Fig 1 right panel). Motion-capture markers were placed on the body to determine the center of mass (CoM) trajectory and joint angles over time.

In our study, the CoM trajectory in Cartesian coordinates during the normal quiet-standing trials (eyes open, standing on a flat rigid surface) for 26 young unimpaired subjects was considered. The CoM was chosen as a

macroscopic representation of overall body behavior; it may be considered equivalent to the end-effector position of an open-kinematic-chain model of upright human posture.

The experimental results for a representative subject are presented in Fig 4. The two panels show: (i) the time trajectories of the CoM position over the 3 trials, and (ii) the related PSD. The x-coordinate of the CoM is presented; the y-coordinate (omitted for clarity) exhibited similar behavior.

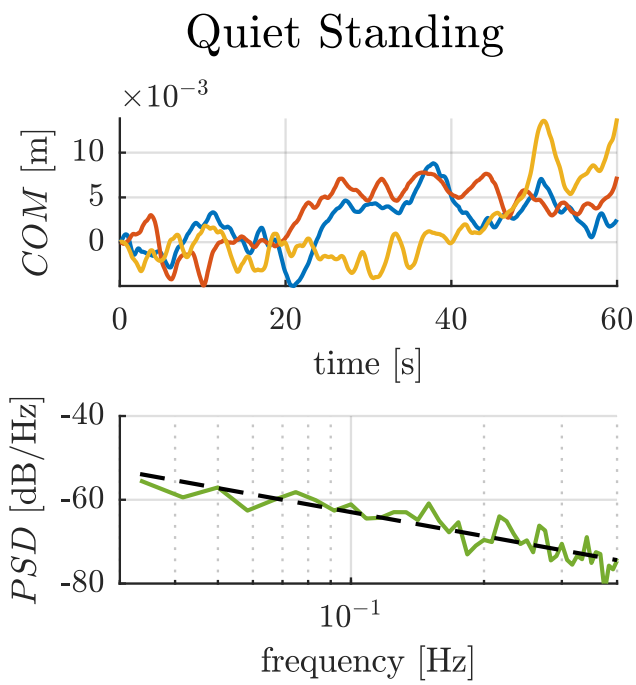

Fig 4. Quiet standing experimental results for a representative subject. Top plot (4.1) shows the 'x' component of the center of mass trajectories over time for multiple trials. The bottom plot (4.2) presents the average power spectral density of 'x' component of the center of mass trajectories (green), while the black dashed line presents the best-fit line with slope -19.05 dB/dec.

The CoM trajectory of the subject (Fig 4.1) shows evidence of random fluctuations. The PSD of these fluctuations follows a linear ($R^2_{PSD} = 0.79$) slope of -19.05 dB/dec in 'x', with 95% CI $[-22.09 \quad -16.00]$ dB/dec, and a slope of -18.27 dB/dec ($R^2_{PSD} = 0.73$) in 'y' with 95% CI $[-21.69 - 14.86]$ dB/dec, over the low-

frequency range (0.03-0.4 Hz) as shown in Fig 4.2. The time trajectory of the signal in Fig 4.1 shows no sign of unboundedness.

A similar behavior was observed across all subjects, with an average slope of -16.06 dB/dec ($R^2_{PSD} = 0.70 \pm 0.14$) with 95% CI on both directions of $[-19.12\ -13.00]$ dB/dec, displaying once again a flatter-than-Brownian slope. The Supplementary Information contain the best-fit PSD slopes, 95% confidence intervals, and coefficients of determination R^2_{PSD} for all subjects.

Descriptive Model

The crank-turning experiments displayed signatures of a purely Brownian process, while the hand-posture experiments showed signs of variance growing linearly with time only up to a certain time point, after which the variance stopped increasing. This observation is consistent with our expectations: position variance must be bounded for postural tasks. However, it is possible that the three tasks share a common control architecture that produces a Brownian process, with an additional layer of control responsible for bounding the variance in postural tasks. Here, we develop a descriptive model assuming that a similar control structure underlies all three tasks.

In a closed-loop negative feedback control system, Brownian behavior in position can emerge from only three sources:

- An additive external disturbance as originally proposed by Peterka [15];
- A free integrator in the closed-loop dynamics;
- A forward-path (reference) velocity command, corrupted by stationary noise and integrated to produce a position reference.

To account for the boundedness of postural tasks (hand posture and quiet standing) the first model (Peterka [15]) assumes a first-order low-pass filter (a ‘leaky integrator’) driven by stationary noise. However, this model

requires a process time-constant on the order of many tens of seconds (80 s), difficult to reconcile with any relevant physiological process. Moreover, that model could not account for the crank-turning data in Fig 2. The second and third models bound the position variance by introducing an intermittent control action. However, the second model would produce a steady-state error between target and measured velocity in the crank-turning task — inconsistent with experimental evidence (Fig 2).

Only the third model, generating Brownian behavior from a forward-path velocity command, could account for all experimental results (Figs 2 to 4). A detailed description of all three models is presented in the Supplementary Information.

A total of 200 numerical simulations per condition were performed to assess the competence of the proposed model to reproduce the experimental observations. Fig 5 shows the model performance in the three different tasks: crank turning, hand posture, and quiet standing.

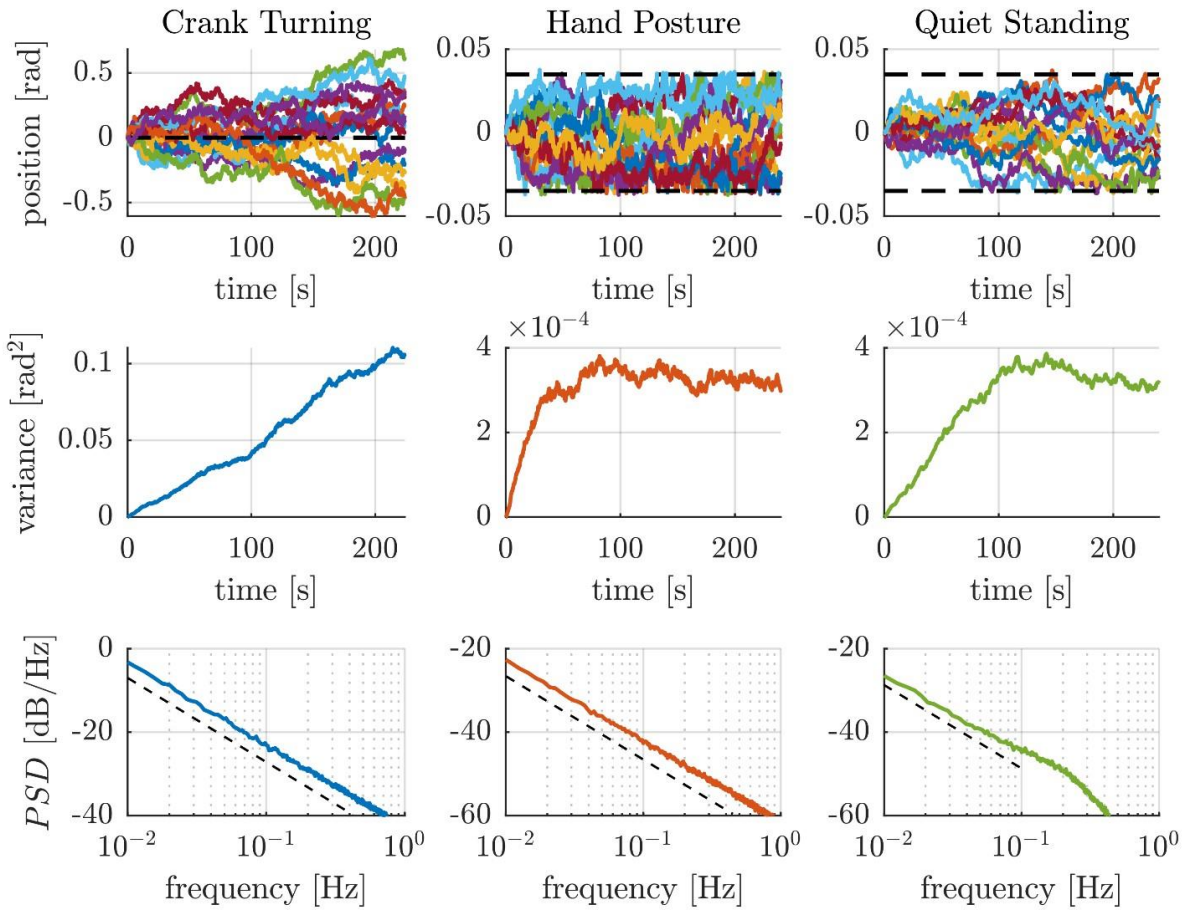

Fig 5. Simulation results of the proposed control model across three tasks: crank turning, hand posture, and quiet standing. The top row of plots shows the time evolution (colored lines) of position relative to the expected nominal trajectory in the three cases; the black dashed line in the crank-turning trajectory plot represents the expected nominal trajectory for the target crank-turning speed, while the black dashed lines in the right two trajectory plots present the thresholds to trigger intermittent control action in the posture control tasks. The middle row of plots shows the variance over time across the ensemble. The bottom row presents the average power spectral densities in the three different tasks. An additional -20 dB/dec dashed-black reference line is added to facilitate interpretation of the results.

The model reproduced both the unbounded Brownian behavior during crank turning (Fig 5 leftmost column) as well as the bounded behavior during hand posture and quiet standing (Fig 5 right two columns). The PSDs (Fig 5 last row) presented a low-frequency (0.01 Hz – 1 Hz for crank turning and hand posture, 0.01 Hz – 0.1 Hz for quiet standing) slope consistent with the experimental evidence: crank-turning: -19.70 dB/dec with 95% CI $[-19.78 \; - 19.61]$ dB/dec; hand posture: -19.42 dB/dec with 95% CI $[-19.50 \; - 19.34]$ dB/dec; and quiet-standing: -17.94 dB/dec with 95% CI $[-18.35 - 17.53]$ dB/dec.

Discussion

A Brownian process – also known as a Wiener process or random walk – is a non-stationary process characterized by variance that grows linearly with time [4]. First discovered by botanist Robert Brown in 1828, it found a more formal definition in one of Einstein's *annus mirabilis* papers in 1905 [4], and was rigorously described mathematically as a stochastic process by Norbert Wiener many years later [3]. Evidence of Brownian processes has been found in many fields: the behavior of particles in a stationary liquid, in chemistry [16], electromagnetism [17], fluid-dynamics [18], and the trends of stock prices [19]. Here we provide evidence that it is a ubiquitous (and perhaps essential) feature of human motor behavior.

Experiments

The experimental PSDs in the crank-turning case show a slope statistically indistinguishable from -20 dB/dec (Fig 2.3). This behavior indicates a strictly Brownian process at low frequencies. In the hand-posture and quiet-standing cases, we observed a flattening of the PSD slope at low frequencies (Figs 3.3 and 4.2). At higher frequencies, the slope varied.

Reaching with the upper limb has been studied widely in motor neuroscience [20–24]. Crank turning has been less widely studied [25–28], despite it being the most common activity of daily living [13]. The crank-turning

task occupies a finite region of the arm's workspace; as a result, the displacement of the hand relative to the thorax is bounded. However, the angular position of the crank is unbounded. Thus, the variance of angular position may grow without bound, and in fact it grew linearly (Fig 2.2), indicating a Brownian process.

The same is not true for postural tasks, such as maintaining a static hand posture and quiet standing. In these cases, a Brownian behavior is still observable in the growing position variance until it reaches a limit (Fig 3.2). This is confirmed by the position trajectories (Figs 3.1 and 4.1) where variance initially grew but was ultimately bounded. All subjects exhibited a transition between approximately linear growth and boundedness, but its onset varied among subjects, ranging from a few seconds to hundreds. Interestingly, a later onset of the bounded behavior corresponded to PSD slopes closer to an unbounded Brownian process (-20 dB/dec), while an earlier onset correlated with flatter PSD slopes.

The existing literature has reported phenomena similar to Brownian motion, often termed "drift" or "sway", in the CoP trajectory during quiet standing. The origin of this "drift" and the underlying human motor control mechanisms have been discussed at length. Collins and De Luca were the first to suggest the presence of "fractional Brownian" behavior in CoP postural sway, proposing an alternation between "do-nothing" (open-loop) and "do-something" (closed-loop) control actions [1]. Thereafter, several studies considered many aspects of this postural "sway": its dependency on sensory information [2], its possible decomposition into different motor control mechanisms [29], the possibility to describe it with linear models [15] or intermittent control [30,31], the kind of stability necessary to explain it [32,33], or the use of different mathematical methods to process it [34–36]. Similar studies were extended to other tasks involving balancing or pointing objects with the upper limbs [5,37]. In these cases, too, related work studied, for example, the influence of sensory information [38] or the underlying control mechanisms [5].

A fractional Brownian process is associated with chaotic dynamics and implies a nonlinear growth of variance with time, unlike the linear growth of variance that characterizes a Brownian process. Our results, however,

indicate no need to postulate fractional behavior. In fact, we believe that the apparent fractional behavior reported in previous work [2,34,35] may be a consequence of the inertial properties of the system and the boundedness of its behavior. A detailed example is presented in the Supplementary Information.

The results reported here establish that a Brownian process is a good description of intrinsic position variability. However, some additional process must act to limit position variance in postural tasks. One possible explanation can be found in the theory of intermittent feedback control. Intermittency in human motor actions has been reported since Woodworth in 1899 [39], and fundamentally arises – in its simplest form – by alternating a "do-nothing" region for small feedback errors within which there is no control action, with "do-something" regions to correct for larger feedback errors. Several studies have supported intermittent control in human motor behavior [1,5,6,30,32,33,40,41].

Models

The proposed descriptive model exhibits Brownian behavior by means of stationary noise added to a reference (forward-path) velocity command. This is equivalent to including a "free integrator" upstream of the interactive dynamics in a Norton equivalent network [42]. To bound the variance in postural tasks, an intermittent controller was included in the forward path where the "do-something" region outside the feedback-error thresholds generated a corrective action encoded as a velocity command. For simplicity, linear representations of the open-loop system dynamics $G(s)$ and compensator $C(s)$ were assumed but that is not essential. We emphasize that this work identified a feature in one of the lowest levels of a complex control system. It is silent about the form of the higher-level controller as long as it presents intermittent feedforward action as velocity commands. Interestingly, this is consistent with recent robotic implementations[43]. Fig 5 shows that this model can reproduce all our experimental observations: crank turning, hand posture, and quiet standing.

This model is not the only possible way to generate a Brownian process in position: there are two alternatives. The first alternative was inspired by Peterka [15] who showed that the phenomena reported by Collins and De Luca [1] could be reproduced by a continuous linear time-invariant controller with a lowpass-filtered stationary noise disturbance, with no need for intermittent ‘open-loop’ and ‘closed-loop’ action.

However, Peterka’s model requires an extremely large filter time-constant (about 80 seconds) to reproduce postural sway, which is difficult to justify for human motor control. Moreover, Peterka’s model cannot reproduce the unbounded variance observed in unbounded tasks, such as crank turning, due to the presence of the leaky integrator of the disturbance signal that will always bound the position variance independent of the task.

A second alternative to obtain a Brownian process in position is to guarantee that the system’s closed-loop transfer function exhibits exactly one pole at zero. In principle, this could be achieved by a controller that compensates exactly for gravitational destabilization during upright posture or by nullifying arm stiffness during gravity-neutral hand posture. Whether intrinsic joint stiffness is sufficient to stabilize standing posture has been debated in the balance literature [44,45]. However, to cancel gravitational stiffness requires less joint stiffness than to stabilize posture and it might be interesting to re-consider this matter in light of this reduced requirement. To maintain gravity-neutral posture of the hand would require imposing a negative stiffness to compensate for intrinsic muscle impedance, which is positive [46,47]. Feedback processes (e.g. via spinal reflexes) could generate ‘negative stiffness’, and apparently do so in some circumstances [48,49].

In this second alternative model, an intermittent control action would suffice to bound the variance in postural tasks. Nonetheless, this model also failed to reproduce the experimental crank-turning data. To guarantee a free-integrator, the second model requires net stiffness equivalent to zero, leading to a steady-state error in velocity and growing error in position. This is not what we observed experimentally.

Of course, it is possible that different control architectures subserve different sensory-motor tasks. However, given the pervasiveness of the linearly-growing variance with time, Brownian behavior appears to be a fundamental feature of neuromotor control that should be considered in future modelling efforts.

In conclusion, a model with forward-path velocity commands corrupted by stationary noise, and intermittent control action during postural tasks, is capable of reproducing all our experimental observations. If the brain encodes descending (forward-path) motor commands in terms of velocity [8–10], because of noise, the resulting position will have to express a Brownian behavior, at least before intermittent correction—just as we observed. To the best of our knowledge, this model, together with the experimental evidence, provides the first known independent behavioral support for the theory of velocity-level planning.

Material and Methods

Subjects

Two different human subject experiments were conducted at MIT: crank turning (10 right-handed college-aged male subjects), and static hand posture control (4 males and 6 females, ages 23-36). All participants gave informed, written consent before the experiment. The informed consent and experimental protocols were reviewed and approved by the Institutional Review Board for the Massachusetts Institute of Technology. The quiet standing data came from a public data set of experiments conducted by Santos et al. (2017), and consisted of data from 49 subjects [14]; the data for the 26 young unimpaired subjects in the study (15 males and 11 females, ages 18-40) were used in this paper.

Crank Turning Experiments

Subjects turned a crank mounted on a high precision incremental optical encoder/interpolator set (Gurley Precision Instruments encoder #8335-11250-CBQA, interpolator #HR2-80QA-BRD) with a resolution of 0.0004 degrees per count.

During the experiment, the subject's arm was occluded from view by a wooden structure, which did not limit the range of motion. The upper arm was suspended by a canvas sling connected to the ceiling using a steel cable; the upper arm and lower arm were in the plane of the crank. The subject sat in a chair with a rigid back, while the shoulder was restrained by a harness attached to the back of the chair. The subject was positioned such that the crank, with radius 10.29 cm, was well within the workspace of the arm. Fig 1 shows a graphical representation of the experimental setup.

The encoder, sampling at 200 Hz, was connected to a set of counters and to the computer via digital I/O. The visual display, also generated by the computer, was on a 17-inch monitor (311 x 238 mm, resolution 1280 x 1024, 76 Hz) which was mounted approximately 75 cm from the subject's eyes. The experiment was divided into two unequal sections: 2 blocks of trials at the subject's preferred or 'comfortable' speed and 6 blocks of trials at a visually-instructed speed.

The data were reported by Hermus et al. [28]. The results presented herein only include analysis of the slow, clockwise-turning condition. However, details of the entire experimental procedure are included for completeness.

At the start of the experiment, subjects performed 20 trials at their preferred speed, 10 trials in the clockwise direction (CW) and 10 in the counterclockwise direction (CCW); both conditions were blocked, in random sequence for each subject; each trial lasted 8 seconds. Subjects were not provided with any visual feedback during these trials. Thereafter, subjects performed 6 blocks of 30 trials, each with visual specification of 1 of 3 target speeds, in either CW or CCW directions. The order of the speed and direction blocks was pseudo-randomized across subjects. The three speeds were selected to cover a significant range: 0.075 rev/s was extremely slow (required over 13 s per

revolution), 0.5 rev/s was close to subjects' preferred speed, and 2.0 rev/s was close to the fastest speed that subjects could turn the crank. Visual feedback on the monitor displayed the target speed, as well as the subject's real-time hand speed; the horizontal axis was time, and the vertical axis was speed. Target speed was displayed as a continuous horizontal line in the middle of the screen. The width of the screen corresponded to the time of the trial. 7 catch trials without visual feedback were included in each block, leaving 23 trials per block with visual feedback.

In the slow-speed conditions, each trial lasted 45 s. This yielded about 3.4 turns of the crank for the slow condition. The duration of the slow-speed trials was chosen as a compromise between acquiring adequate data and avoiding subject fatigue. The first and last cycle were removed to eliminate transients. This yielded a 26-second trial duration for analysis. The first 2 trials of each block were considered to be familiarization trials, and were thus removed together with the 7 catch trials without visual feedback, leaving 21 trials per subject for analysis.

Hand Posture Experiments

In the hand posture experiment, subjects were asked to hold the handle of an InMotion2 robot (Interactive Motion Technologies Inc.) and maintain a static hand posture at the center of a circle of radius 2.5 cm. The InMotion2 is a highly back-drivable two-link manipulandum. In the experiments, the robot served only as a position measurement device as the actuators were open-circuited. InMotion joint positions were measured by a 16-bit/rev encoder at ~350 Hz using a Compact RIO real-time processor. Data were interpolated to a sampling rate of 200 Hz.

The experimental setup was the same as the previous crank experiment except that the crank was replaced with the InMotion2 robot, vision of the hand was not occluded, and the visual feedback was changed to show the fixed target position (given by a circle of radius 2.5 cm) and the subject's actual hand position (given by a dot of radius 1 cm). Fig 1 shows the experimental configuration. Each trial lasted 4 minutes, and was repeated 10 times for each subject, with breaks between trials.

Quiet Standing Experiments

The quiet standing experiments were conducted by Santos et al. (2017) in the Laboratory of Biomechanics and Motor Control at the Federal University of ABC, Brazil [14]. Subjects were asked to stand barefoot, as still as possible, with their arms by their sides, under four conditions: on a rigid surface with eyes open, on a rigid surface with eyes closed, on a compliant surface (foam blocks) with eyes open, and on a compliant surface with eyes closed. Trials lasted 60 s and were performed 3 times per condition in random order. 3D kinematics were measured using a motion capture system, with data sampled at 100 Hz; post-processing was performed to estimate the center of mass (CoM) trajectory in Cartesian coordinates, as well as joint angles. Fig 1 shows the experimental configuration. Further experimental details can be found in the article by Santos et al. (2017) [14].

The results presented herein include data for the first condition (eyes open, rigid surface), and for the 26 young unimpaired subjects. The estimated CoM trajectories included in the public data set were used in the data analysis. Note that the chosen (x,y,z) coordinate directions (see Fig 1) are different from those used in the public data set by Santos et al. This was done to have the (x,y) coordinates laying in the horizontal plane for both quiet standing and hand posture.

Data Analysis

The data - crank angular position, hand position (x,y), and CoM position (x,y) - were processed using MATLAB (version 2022a). Three different quantities were analyzed: (i) the time trajectory of the position data over each trial, (ii) their variance-over-time computed across the ensemble, and (iii) their average power spectral density.

The time trajectory was directly extracted from each trial of the collected data. For all research studies (crank turning, hand posture, and quiet standing), data from all trials were aligned such that the initial data point was taken to be at the origin, namely $0\ rad$ for the crank turning angle, and $(0,0)\ m$ for the hand and CoM Cartesian coordinates.

The variance across the ensemble was computed at each time step ($t_s = 0.005\ s$) using the time trajectories (aligned at the initial data point) with the following equation:

$$\sigma^2(t) = \frac{1}{N-1}\sum_{i=1}^{N}\left(x(i,t) - \frac{1}{N}\sum_{j=1}^{N} x(j,t)\right)^2$$

where i and j represent the trial indices ranging from 1 to N (number of trials), and $x(i,t)$ represents the value of the considered variable at time t during the i-th trial.

The power spectral densities (PSDs) were computed for each trial with Welch's method (*50*) using each entire trial as one window of data (in order to obtain spectral estimates down to the lowest possible frequency) and averaging across trials. The data were pre-processed by removing the average crank angle trajectory from the crank angle data, and removing the mean position over each trial for the hand position and CoM position data. The PSDs were post-processed to remove the lowest-three frequency points, as these depended sensitively on the data processing technique used (see the Supplementary Information for details of the pre- and post-processing decisions).

Modeling

The descriptive mathematical model, represented in the block diagram of Fig 6, was implemented in Simulink/MATLAB (v 2022a) to simulate the behavior of the three different motor tasks: crank turning, hand posture, and quiet standing. For each of these cases, a single-degree-of-freedom model was considered for simplicity.

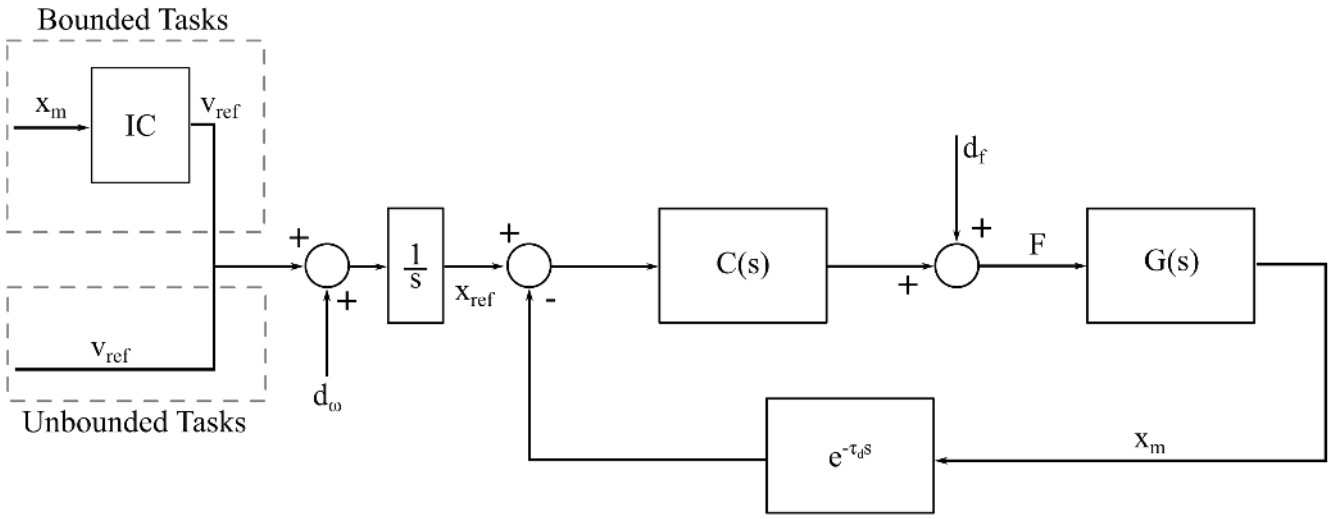

Fig 6. Block diagram of the modelled control scheme. G(s) represents the open-loop system dynamics, where s is the Laplace variable; C(s) is the closed-loop control action; IC represents the intermittent controller necessary to bound position variance; d_f and d_ω represent additive noise on the control action (force/torque) and on the reference velocity command, respectively; τ_d represents sensor delay; F is the control action; x_{ref} is the reference position; and v_{ref} is the reference speed.

Additive disturbance sources were included at the reference motion command and at the control action, denoted as d_ω and d_f respectively. Both disturbances were modeled as white noise. A constant delay of $\tau_d = 100\ ms$ was included in the feedback path to account for feedback delays in the human sensorimotor system. The results were robust to decreasing the delay τ_d; if τ_d was set to zero the same results were observed.

An idealized transfer function for the linearized open-loop system $G(s)$, where s is the Laplace variable, was designed to represent two configurations: a gravity-neutral arm $G_{arm}(s)$ or upright stance $G_{stance}(s)$:

- $G_{arm}(s) = \frac{1}{mL^2s^2+\beta s}$

- $G_{stance}(s) = \frac{1}{mL^2s^2+\beta s-mgL}$

In the gravity-neutral-arm case, the system dynamics $G_{arm}(s)$ represents a marginally stable 2nd order linear-time-invariant (LTI) system, with moment-of-inertia mL^2 and damping factor β, where m is the total mass of the arm, and L is the distance between the shoulder joint and the center of mass (CoM) of the arm. The distributed moment of inertia was neglected.

In the quiet-standing case, the system dynamics $G_{stance}(s)$ represents an unstable 2nd-order LTI system i.e., an inverted pendulum, with moment of inertia mL^2, damping factor β, and destabilizing gravitational stiffness mgL, where m is the total mass of a human body, L is the distance between the ankle joint and center of mass (CoM) of the whole body, and g is the gravitational acceleration (9.81 m/s^2). Again, the distributed moment of inertia was neglected.

The closed-loop dynamics controller $C(s)$ was designed to guarantee asymptotic stability of the closed-loop transfer function. Specifically,

- For the gravity-neutral arm, we set $C(s) = k_c > 0$;
- For upright posture, we set $C(s) = k_c > mgL$.

In static hand posture and quiet stance, an additional intermittent controller (IC) was introduced to bound the otherwise unbounded Brownian behavior. The chosen intermittent control performed no control action within the "do-nothing" region, while it generated a Gaussian velocity profile whenever the actual position measurement (x_m) was outside the threshold of the "do-nothing" region. From a mathematical point of view, this was represented by the following control law:

$$v_{ref}(t) = \begin{cases} 0 & if \quad -x_{th} \leq x_m(t) \leq +x_{th} \\ v_{max}e^{-\frac{(t-t_0)^2}{2c^2}} & if \quad x_m(t) < -x_{th} \vee x(t) > +x_{th} \end{cases}$$

where v_{max} represents the peak velocity of the control command, t_0 is the timing offset, and c is the standard deviation of the Gaussian profile. This intermittent control was based on the theory of dynamic motor primitives, and velocity-coded submovements specifically (*46*). However, other control architectures that include intermittency, with a "do-nothing" region and a "do-something" region, would produce equivalent results as long as the "do-something" region included a sufficient corrective action to push the controlled system back into the "do-nothing" region.

200 simulations of this model were performed for each of the three motion tasks. The noise disturbance profiles were generated with pseudo-random white-noise sequences, initialized with different seeds to guarantee independence between the different simulations. Table 1 summarizes the values of the parameters used for the simulations. In each motor task, the position trajectory over time was sampled at a frequency of 100 Hz and then processed using the same data analysis methodology adopted for the experimental data.

Table 1. Parameters used in the simulations of the two considered cases: upper-extremity gravity-neutral arm posture and upright stance.

Parameter	Upper-Extremity Gravity-Neutral Arm Posture	Upright Standing Balance
m	1.5 kg	75 kg
β	30 Nms/rad	226 Nms/rad
L	0.35 m	1 m
k_c	65 Nm/rad	883 Nm/rad

Acknowledgments

We would like to thank the members of the Newman Laboratory for Biomechanics and Human Rehabilitation for the continuous support and valuable feedback throughout this research project.

The authors contributed to the different parts of this work in the following way (FT: Federico Tessari, JH = James Hermus, RSD = Rika Sugimoto-Dimitrova, NH = Neville Hogan):

- Conceptualization: FT, JH, RSD, NH
- Methodology: FT, JH, RSD, NH
- Investigation: FT, JH, RSD
- Visualization: FT, JH, RSD
- Funding acquisition: NH
- Project administration: NH
- Supervision: NH
- Writing – original draft: FT
- Writing – review & editing: FT, JH, RSD, NH

References

1. Collins JJ, De Luca CJ. Open-loop and closed-loop control of posture: A random-walk analysis of center-of-pressure trajectories. Exp Brain Res. Springer-Verlag; 1993.

2. Collins JJ, De Luca CJ. The effects of visual input on open-loop and closed-loop postural control mechanisms. Exp Brain Res. 1995;103: 151–163.

3. Wiener N. Norbert Wiener: Collected Works: Mathematical Philosophy and Foundations; Potential Theory; Brownian Movement, Wiener Integrals, Ergodic and Chaos Theories, Turbulence and Statistical Mechanics. Masani P, editor. 1976;1: 760.

4. Einstein A. On the movement of small particles suspended in stationary liquids required by the molecular-kinetic theory of heat. Ann Phys. 1905;17: 549–560.

5. Cabrera JL, Milton JG. On-off intermittency in a human balancing task. Phys Rev Lett. 2002;89: 158702. doi:10.1103/PhysRevLett.89.158702

6. Gawthrop P, Loram I, Lakie M, Gollee H. Intermittent control: A computational theory of human control. Biol Cybern. 2011;104: 31–51. doi:10.1007/S00422-010-0416-4/METRICS

7. Inoue Y, Mao H, Suway SB, Orellana J, Schwartz AB. Decoding arm speed during reaching. Nature Communications 2018 9:1. 2018;9: 1–14. doi:10.1038/s41467-018-07647-3

8. Schwartz AB. Direct Cortical Representation of Drawing. Science (1979). 1994;265: 540–542. doi:10.1126/SCIENCE.8036499

9. Moran DW, Schwartz AB. Motor cortical representation of speed and direction during reaching. J Neurophysiol. 1999;82: 2676–2692. doi:10.1152/JN.1999.82.5.2676/ASSET/IMAGES/LARGE/9K1090522015.JPEG

10. Schwartz AB. Motor cortical activity during drawing movements: population representation during sinusoid tracing. https://doi.org/101152/jn199370128. 1993;70: 28–36. doi:10.1152/JN.1993.70.1.28

11. Churchland MM, Yu BM, Ryu SI, Santhanam G, Shenoy K v. Neural Variability in Premotor Cortex Provides a Signature of Motor Preparation. Journal of Neuroscience. 2006;26: 3697–3712. doi:10.1523/JNEUROSCI.3762-05.2006

12. Shenoy K v., Sahani M, Churchland MM. Cortical Control of Arm Movements: A Dynamical Systems Perspective. https://doi.org/101146/annurev-neuro-062111-150509. 2013;36: 337–359. doi:10.1146/ANNUREV-NEURO-062111-150509

13. Petrich L, Jin J, Dehghan M, Jagersand M. A Quantitative Analysis of Activities of Daily Living: Insights into Improving Functional Independence with Assistive Robotics. Proc IEEE Int Conf Robot Autom. 2022; 6999–7006. doi:10.1109/ICRA46639.2022.9811960

14. dos Santos DA, Fukuchi CA, Fukuchi RK, Duarte M. A data set with kinematic and ground reaction forces of human balance. PeerJ. 2017;2017: e3626. doi:10.7717/PEERJ.3626/SUPP-2

15. Peterka RJ. Postural control model interpretation of stabilogram diffusion analysis. Biol Cybern. 2000;82: 335–343.

16. Kramers HA. Brownian motion in a field of force and the diffusion model of chemical reactions. Physica. 1940;7: 284–304. doi:10.1016/S0031-8914(40)90098-2

17. Kurşunoğlu B. Brownian motion in a magnetic field. Ann Phys (N Y). 1962;17: 259–268. doi:10.1016/0003-4916(62)90027-1

18. Hauge EH, Martin-Löf A. Fluctuating hydrodynamics and Brownian motion. Journal of Statistical Physics 1973 7:3. 1973;7: 259–281. doi:10.1007/BF01030307

19. Osborne MFM. Brownian Motion in the Stock Market. https://doi.org/101287/opre72145. 1959;7: 145–173. doi:10.1287/OPRE.7.2.145

20. Gulletta G, Erlhagen W, Bicho E. Human-Like Arm Motion Generation: A Review. Robotics 2020, Vol 9, Page 102. 2020;9: 102. doi:10.3390/ROBOTICS9040102

21. Burdet E, Osu R, Franklin DW, Milner TE, Kawato M. The central nervous system stabilizes unstable dynamics by learning optimal impedance. Nature 2001 414:6862. 2001;414: 446–449. doi:10.1038/35106566

22. Flash T, Hogan N. The coordination of arm movements: an experimentally confirmed mathematical model. Journal of Neuroscience. 1985;5: 1688–1703. doi:10.1523/JNEUROSCI.05-07-01688.1985

23. Abend W, Bizzi E, Morasso P. Human arm trajectory formation. Brain. 1982;105: 331–348. doi:10.1093/BRAIN/105.2.331

24. Won J, Hogan N. Stability properties of human reaching movements. Exp Brain Res. 1995;107: 125–136. doi:10.1007/BF00228024/METRICS

25. Russell D, Hogan N. Dealing with constraints: a biomechanical approach. Images of the Twenty-First Century Proceedings of the Annual International Engineering in Medicine and Biology Society. IEEE; 1989. pp. 892–893. doi:10.1109/IEMBS.1989.96034

26. Ohta K, Svinin MM, Luo Z, Hosoe S, Laboissière R. Optimal trajectory formation of constrained human arm reaching movements. Biol Cybern. 2004;91: 23–36. doi:10.1007/s00422-004-0491-5

27. Hermus J, Sternad D, Hogan N. Evidence for dynamic primitives in a constrained motion task. 2020 8th IEEE RAS/EMBS International Conference for Biomedical Robotics and Biomechatronics (BioRob). IEEE; 2020. pp. 551–556. doi:10.1109/BioRob49111.2020.9224352

28. Hermus J, Doeringer J, Sternad D, Hogan N. Separating neural influences from peripheral mechanics: The speed-curvature relation in mechanically constrained actions. J Neurophysiol. 2020;123: 1870–1885. doi:10.1152/JN.00536.2019/ASSET/IMAGES/LARGE/Z9K0042054220012.JPEG

29. Zatsiorsky VM, Duarte M. Instant Equilibrium Point and its Migration in Standing Tasks: Rambling and Trembling Components of the Stabilogram. Motor Control. 1999;3: 28–38.

30. Morasso P, Cherif A, Zenzeri J. State-space intermittent feedback stabilization of a dual balancing task. Sci Rep. 2020;10. doi:10.1038/s41598-020-64911-7

31. Loram I, Gollee H, Kamp C van de, Gawthrop P. Is intermittent control the source of the non-linear oscillatory component (0.2-2Hz) in human balance control. IEEE Trans Biomed Eng. 2022. doi:10.1109/TBME.2022.3174927

32. Bottaro A, Casadio M, Morasso PG, Sanguineti V. Body sway during quiet standing: Is it the residual chattering of an intermittent stabilization process? Hum Mov Sci. 2005;24: 588–615. doi:10.1016/j.humov.2005.07.006

33. Bottaro A, Yasutake Y, Nomura T, Casadio M, Morasso P. Bounded stability of the quiet standing posture: An intermittent control model. Hum Mov Sci. 2008;27: 473–495. doi:10.1016/J.HUMOV.2007.11.005

34. Delignières D, Torre K, Bernard PL. Transition from persistent to anti-persistent correlations in postural sway indicates velocity-based control. PLoS Comput Biol. 2011;7. doi:10.1371/journal.pcbi.1001089

35. Kuznetsov N, Bonnette S, Gao J, Riley MA. Adaptive fractal analysis reveals limits to fractal scaling in center of pressure trajectories. Ann Biomed Eng. 2013;41: 1646–1660. doi:10.1007/s10439-012-0646-9

36. Hernandez ME, Snider J, Stevenson C, Cauwenberghs G, Poizner H. A Correlation-Based Framework for Evaluating Postural Control Stochastic Dynamics. IEEE Transactions on Neural Systems and Rehabilitation Engineering. 2016;24: 551–561. doi:10.1109/TNSRE.2015.2436344

37. Goh S, Han K, Ryu J, Kim S, Choi MY. Failure of arm movement control in stroke patients, characterized by loss of complexity. PLoS One. 2015;10. doi:10.1371/journal.pone.0141996

38. Brown LE, Rosenbaum DA, Sainburg RL. Limb Position Drift: Implications for Control of Posture and Movement. J Neurophysiol. 2003;90: 3105–3118. doi:10.1152/JN.00013.2003/ASSET/IMAGES/LARGE/9K1133531010.JPEG

39. Woodworth RS. Accuracy of voluntary movement. The Psychological Review: Monograph Supplements. 1899;3: i–114. doi:10.1037/H0092992

40. Markkula G, Boer E, Romano R, Merat N. Sustained sensorimotor control as intermittent decisions about prediction errors: computational framework and application to ground vehicle steering. Biol Cybern. 2018;112: 181–207. doi:10.1007/s00422-017-0743-9

41. CRAIK KJW. THEORY OF THE HUMAN OPERATOR IN CONTROL SYSTEMS1. British Journal of Psychology General Section. 1947;38: 56–61. doi:10.1111/J.2044-8295.1947.TB01141.X

42. Hogan N. Physical interaction via dynamic primitives. Springer Tracts in Advanced Robotics. 2017;117: 269–299. doi:10.1007/978-3-319-51547-2_12/FIGURES/7

43. Hwangbo J, Lee J, Dosovitskiy A, Bellicoso D, Tsounis V, Koltun V, et al. Learning agile and dynamic motor skills for legged robots. Sci Robot. 2019;4. doi:10.1126/SCIROBOTICS.AAU5872/SUPPL_FILE/AAU5872_SM.PDF

44. Winter DA, Patla AE, Rietdyk S, Ishac MG. Ankle Muscle Stiffness in the Control of Balance During Quiet Standing. 2001 [cited 20 Dec 2022]. Available: www.jn.org

45. Loram ID, Lakie M. Direct measurement of human ankle stiffness during quiet standing: The intrinsic mechanical stiffness is insufficient for stability. Journal of Physiology. 2002;545: 1041–1053. doi:10.1113/JPHYSIOL.2002.025049

46. Mussa-Ivaldi FA, Hogan N, Bizzi E. Neural, mechanical, and geometric factors subserving arm posture in humans. Journal of Neuroscience. 1985;5: 2732–2743. doi:10.1523/JNEUROSCI.05-10-02732.1985

47. Bennett DJ, Hollerbach JM, Xu Y, Hunter IW. Time-varying stiffness of human elbow joint during cyclic voluntary movement. Exp Brain Res. 1992;88: 433–442. doi:10.1007/BF02259118/METRICS

48. Gillard DM, Yakovenko S, Cameron T, Prochazka A. Isometric muscle length–tension curves do not predict angle–torque curves of human wrist in continuous active movements. J Biomech. 2000;33: 1341–1348. doi:10.1016/S0021-9290(00)00127-5

49. Gillard DM, Yakovenko S, Cameron T, Prochazka A. Torque-angle relationships of human wrist muscles. Annual International Conference of the IEEE Engineering in Medicine and Biology - Proceedings. 1999;1: 554. doi:10.1109/IEMBS.1999.802632

50. Solomon, Jr, O M., PSD computations using Welch's method, Sandia Report, (1991).

Supporting Information

Spectral Analysis

Power spectral densities (PSDs) were computed for each data set using Welch's method [50]. Various pre-processing techniques were applied to the data were compared with the goal of reducing any numerical artifacts in the computed PSDs. Three different detrending approaches were considered: (I) no detrending, (II) subtraction of the mean, and (III) linear detrending. Furthermore, two windows were tested on the data: (I) rectangular window, and (II) Hanning window. Fig S1 shows PSDs computed using different detrending and windowing approaches for one subject performing the hand posture task. The different approaches mainly affected the three lowest-frequency data points, which were therefore removed from the reported PSDs. The window shape mainly affected the total signal power, without significantly affecting the shape of the spectrum. This can be explained by the fact that the Hanning window is used to taper the ends of the data window, effectively reducing signal amplitude. The Hanning window is typically used to obtain cleaner high frequency spectral estimates, reducing side-lobe artifacts that may be *produced* by other windowing methods, including the rectangular window. Since we were interested in the low-frequency spectrum, which is largely unaffected by the choice of the window, the final PSDs were computed using the rectangular window as it involved minimal processing of the data.

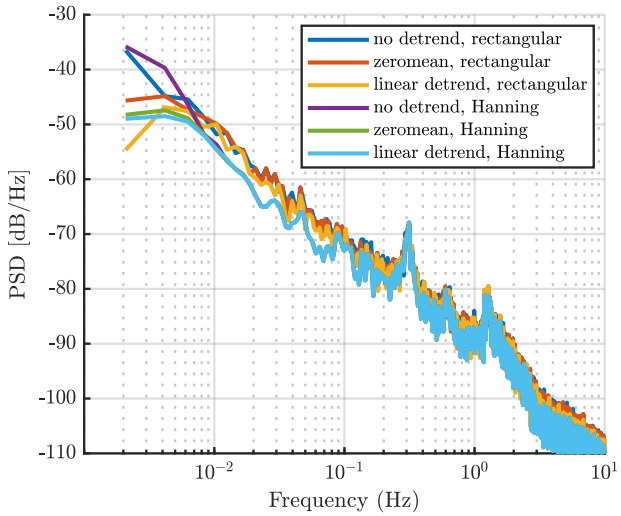

S1 Fig. Power spectral densities for a single subject performing the hand posture experiment. They were computed using six different pre-processing techniques: no detrending with rectangular window (blue), zero-mean with rectangular window (red), linear detrend with rectangular window (yellow), no detrending with Hanning window (purple), zero-mean with Hanning window (green), linear detrend with rectangular window (light blue). The detrending process mainly affects the lowest-frequency data points, while the window shape affects total signal power.

For the crank-turning task, which involved displacements due to voluntary movement of the hand around the crank, the crank-angle data were detrended by removing the average trajectory over the 21 trials in order to focus the spectral analysis on the random fluctuations around the average trajectory.

Alternative Models

Two alternative models were investigated to describe a Brownian process in position emerging from a closed-loop negative feedback control system. The first was based on work proposed by Peterka [15], where stationary noise is filtered through a low-pass filter with an extremely low cut-off frequency, a so-called ‘leaky integrator’, and injected as a disturbance into the feedback control loop. Stationary noise filtered through a ‘leaky

integrator' generates a Brownian-like behavior that is bounded, with variance growing linearly over time until the low cut-off frequency of the filter is reached. Such a model reproduces the Brownian-like behavior observed in postural tasks, such as hand posture control or quiet standing, in which the variance is bounded. However, it fails to reproduce the unbounded Brownian behavior of velocity-based tracking tasks, such as turning a crank.

A second alternative model describes the Brownian behavior in position as emerging from the closed-loop dynamics. In this case the closed-loop transfer function requires exactly one pole at the complex-plane origin i.e., a free integrator. The controller required to produce this behavior differs depending on the open-loop dynamics G(s) of the system being considered, which can be:

I. unstable (at least one pole with positive real part);

II. asymptotically stable (all poles with negative real parts);

III. marginally/neutrally stable (one pole at the origin).

For cases (I) and (II), the controller $C(s)$ was designed to cancel all unstable poles, and place one pole at the origin. In case (III), the open-loop system already presents a pole at the origin, so the controller $C(s)$ was designed such that the pole at the origin was not shifted. Consider three different 2nd order LTI systems e.g., mass-spring-damper systems, with $G(s)$ in each of the three previously mentioned cases, and the corresponding controller $C(s)$ required to place a single closed-loop pole at the origin:

I. If $G(s) = \frac{1}{ms^2+\beta s-k}$, then $C(s) = k_c = k$

II. If $G(s) = \frac{1}{ms^2+\beta s+k}$, then $C(s) = k_c = -k$

III. If $G(s) = \frac{1}{ms^2+\beta s}$, then $C(s) = k_c = 0$

The 2nd alternative model, with the three variations described above to produce a free integrator, would guarantee the appearance of an unbounded Brownian behavior in position. To bound the Brownian behavior in postural tasks (hand posture and quiet standing), an intermittent controller was designed such that the control actions producing the free integrator were augmented to limit the position variance. In the postural tasks, the condition was a threshold in the position error: when the position error was within the thresholds, the closed-loop dynamics maintained a pole at the origin, while when the error exceeded the thresholds, the closed-loop dynamics exhibited an asymptotically stable behavior. Fig S2 presents a possible intermittent control action $C(s)$ for the three considered open-loop dynamics: unstable, asymptotically stable, and marginally stable.

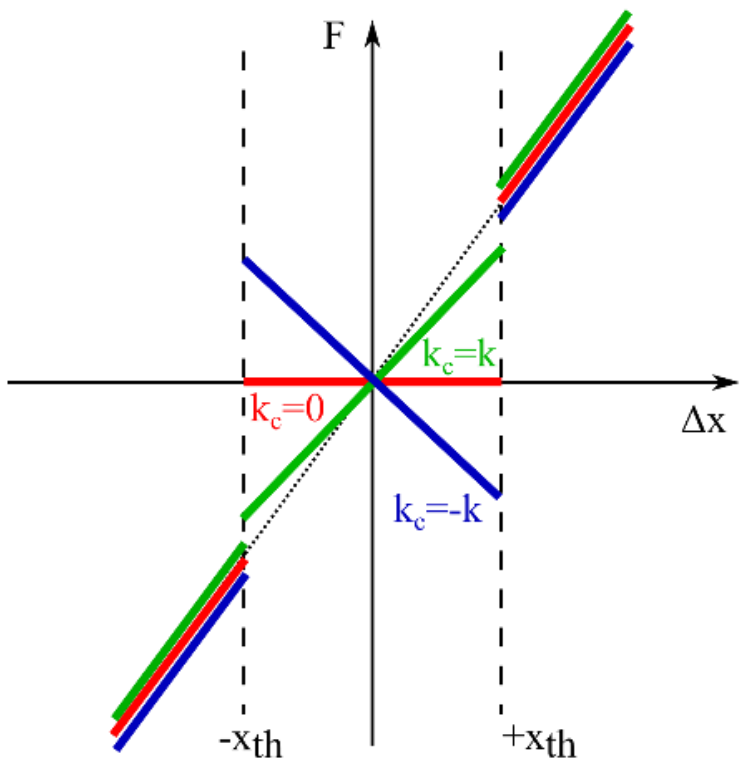

S2 Fig. Intermittent control action based on position thresholds $\pm x_{th}$ (black dashed lines). It is designed to guarantee a free integrator in the closed-loop dynamics when the error is within the thresholds for three different

open-loop dynamics: unstable (green solid line), marginally stable (red line), asymptotically stable (blue). Outside the thresholds the controller guarantees an asymptotically stable behavior.

Stabilogram Diffusion Analysis

Stabilogram diffusion analysis was introduced by Collins and De Luca to study the fluctuations observed in the trajectory of the center of pressure (CoP) position during quiet stance [1]. It is a time-series analysis tool borrowed from statistical mechanics that involves computing the mean-squared displacement (MSD) of a signal for different time intervals to analyze the nature of the fluctuations present in the time series.

Consider a signal sequence $x(k)$ with $k = 1, \dots, N$, and let Δt denote the span interval between two points of the $x(k)$ data sequence. The mean-squared displacement can be computed as:

$$\Delta r^2(\Delta t) = \frac{\sum_{k=1}^{N-\Delta t}\left(x(k+\Delta t) - x(k)\right)^2}{N - \Delta t}$$

The mean-squared displacement can then be plotted with respect to different span intervals Δt to produce a diffusion plot. The evolution of Δr^2 provides information on the fractality of the analyzed time series. In fact, it is known that a fractional random walk process is characterized by the following relationship between the mean-squared displacement and time:

$$\Delta r^2 \sim \Delta t^{2H}$$

where the scaling exponent H denotes the Hurst coefficient, and can be obtained from a log-log plot of Δr^2 with respect to Δt. When the slope 2H is exactly equal to 1, corresponding to $H = 0.5$, the behavior follows a classical (purely) Brownian process, with variance that grows linearly with time. Instead, if $H \neq 0.5$, the process is classified as a fractal or "fractional Brownian" process, which can be persistent ($H > 0.5$) or anti-persistent ($H < 0.5$) [1].

Collins and De Luca observed that their diffusion plots exhibited two distinct regions with different slopes: what they referred to as a "short-term" region and a "long-term" region. The slopes measured in the log-log diffusion plots suggested the presence of "fractional Brownian" processes in both regimes, with persistent behavior in the short term, and anti-persistent behavior in the long term. Furthermore, the change in slope, from a persistent to an anti-persistent regime, was interpreted as a sign of intermittent control. However, it is important to observe that the system considered here is an inertial system, and that may account for higher-order trends manifest in the diffusion plot, including a change in the observed slope. By means of numerical simulations in MATLAB, we observed – Fig S3 – that it is possible to reproduce a diffusion plot like that of Collins and De Luca, with two regions with different slopes.

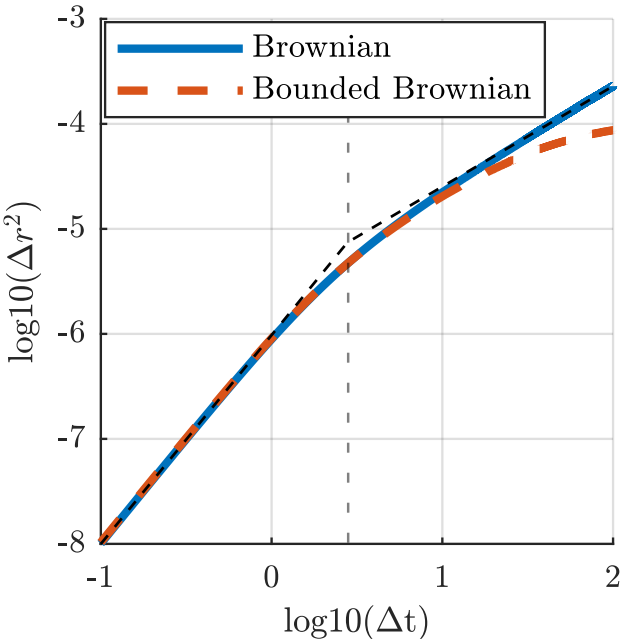

S3 Fig. Diffusion plots of a Brownian process (blue line) and of a bounded Brownian process (dashed red line). Both were filtered through a second order mechanical system. The vertical dashed grey line indicates the critical point that divides the short-term and long-term regions with different slopes. The black dashed lines represent the best-fit lines before and after the critical point.

We considered two different inputs: (i) a purely Brownian input and (ii) a bounded Brownian input, obtained by bounding the Brownian process. We then injected these noise sources into a 2nd order dynamical system comprising a mass, spring and damper. The results – presented in Fig S2 – show the average of 100 simulations performed considering a pseudo-random white noise source with randomized initial seed integrated to obtain a purely Brownian time series that was filtered through a 2nd order mechanical system with the following properties: 75 kg mass, 245 Ns/m damping factor and 200 N/m stiffness. When we consider a purely Brownian process input (blue line of Fig S3), the slope of the long-term region is exactly 1, corresponding to $H = 0.5$. On the other hand, when a bounded Brownian input (dashed red line of Fig S3) was injected in the system, the slope of the long-term region decreased such that $H < 0.5$. The slope of short-term region was 2 ($H = 1$) with both inputs (purely Brownian and bounded Brownian), and likely arose from the inertial dynamics, which is expected to exhibit "persistent" behavior. These results also agree with the spectral analysis of the experimental data: the Brownian process dominates at lower frequencies (long time scales), with flatter slopes observed when the process is bounded.

Confidence Intervals

A linear regression model was used to fit the low-frequency region of the PSDs of the analyzed motor tasks. The linear regression was performed in the log-log plane. For each subject a best-fit slope m_{sl} [dB/dec] and a best-fit intercept q_{sl} [dB] was identified such that:

$$PSD = m_{sl} \cdot f + q_{sl}$$

Additionally, for each regression line, the coefficient of determination R^2 was computed to assess how well a linear model fit the low-frequency data.

The confidence intervals (CI) on the identified slope m_{sl} of the PSD were computed using the following equation:

$$CI = m_{sl} + t([\alpha, 1-\alpha], N-2) \cdot \left(\frac{\sigma}{\sqrt{N-2}}\right)$$

$$\alpha = \frac{1}{2}\frac{100 - CI_{target}}{100}$$

where $t([\alpha, 1-\alpha], N-2)$ represents the t-score cumulative distributed function values for a confidence range of α. N represents the number of samples, while σ is the standard deviation of the slope [dB/dec]. We set the confidence interval target at $CI_{target} = 95\%$.

The standard deviation of the slope σ was computed as:

$$\sigma = \sqrt{\frac{\sum_{i=1}^{N}\left(PSD_m(i) - PSD_e(i)\right)^2}{\sum_{i=1}^{N}\left(\log_{10} f_m(i)\ _m - mean(\log_{10} f_m(i))\right)^2}}$$

where PSD_m is the measured power spectral density, PSD_e is the estimated power spectral density obtained from the linear regression model, and f_m is the measured frequency.

The data presented in the main text showed the performance of only one subject for each analyzed condition. Here we report the 95% confidence intervals (CIs) for the identified slope m_{sl} for the power spectral densities of each subject for each motor tasks: crank turning (Fig S4), hand posture (Fig S5), and quiet standing (Fig S6). Moreover, Table S1, Table S2 and Table S3 report respectively the R^2 coefficients for the PSD linear fitting of crank turning, hand posture and quiet standing.

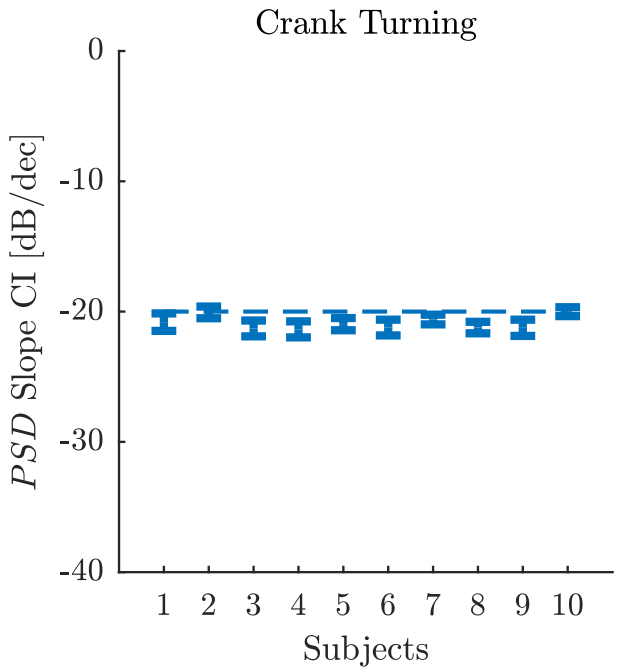

S4 Fig. Confidence Intervals (CI) of best-fit slope for the PSD of the crank angular position for each tested subject during the crank-turning experiment.

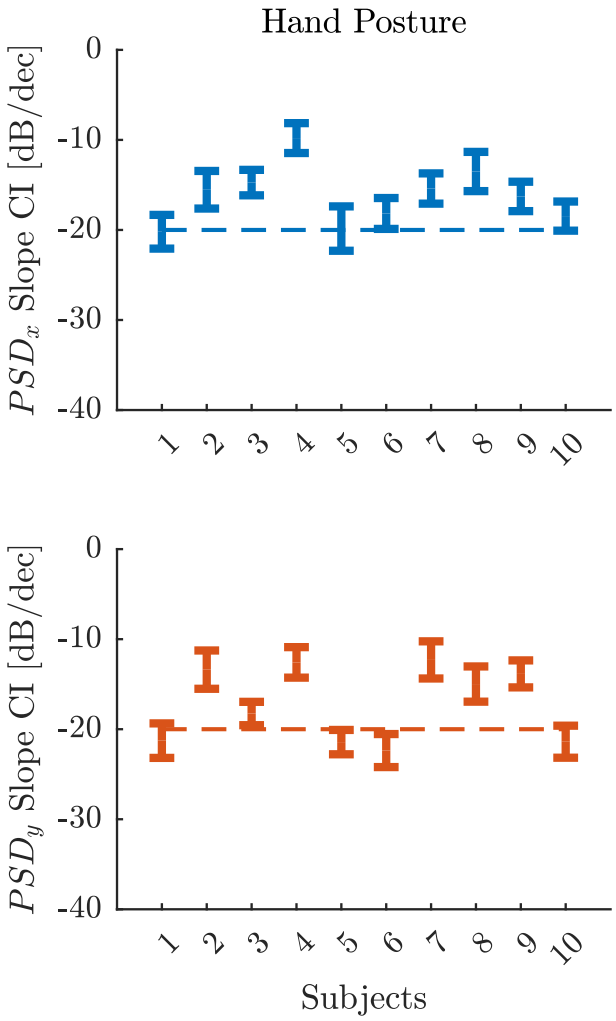

S5 Fig. Confidence Intervals (CI) of the best-fit slope for the PSD of the hand Cartesian position for each tested subject during the hand-posture experiment. The top chart shows the 'x' component of the hand trajectory, while bottom chart shows the 'y' component of the hand trajectory.

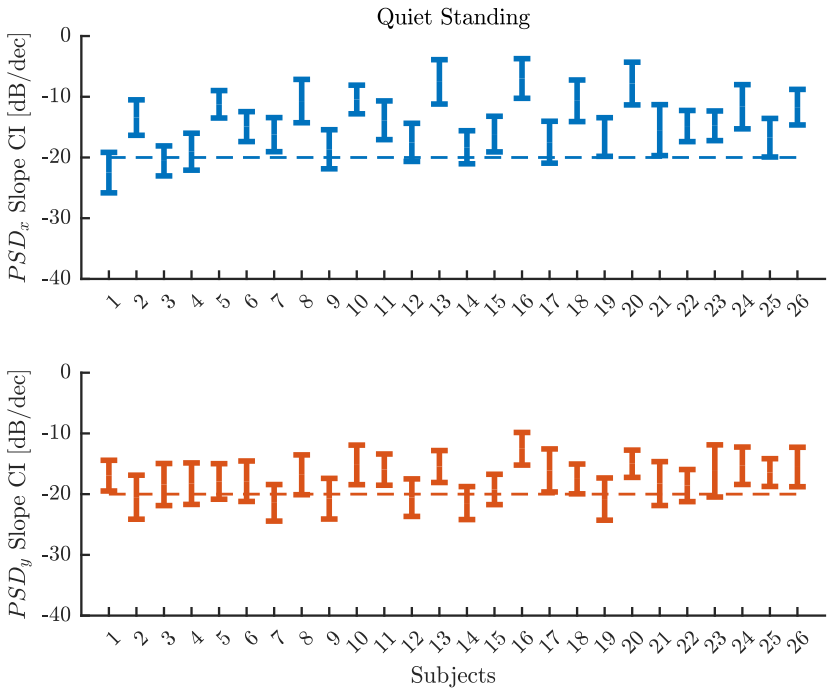

S6 Fig. Confidence Intervals (CI) of the best-fit slope for the PSD of the center of mass (CoM) trajectory for each tested subject during the quiet standing experiment. The top chart shows the 'x'-component of the CoM position, while bottom chart shows the 'y'-component of the CoM position.

S1 Table. Linear regression R^2 coefficients of the low-frequency PSD fit during crank turning in different subjects.

Subject	*PSD – Linear Regression R^2*
1	0.988
2	0.994
3	0.991
4	0.990
5	0.994
6	0.991
7	0.996
8	0.995
9	0.990
10	0.997
TOT	0.993±0.003

S2 Table. Linear regression R^2 coefficients of the low-frequency PSD fit during hand posture in the different subjects for both 'x' and 'y' directions.

Subject	*Direction*	*PSD – Linear Regression R^2*
1	x	0.92
	y	0.92
2	x	0.80
	y	0.74
3	x	0.92
	y	0.95
4	x	0.65
	y	0.75
5	x	0.87
	y	0.96
6	x	0.92
	y	0.94
7	x	0.86
	y	0.72
8	x	0.79
	y	0.85
9	x	0.91
	y	0.89
10	x	0.93
	y	0.94
TOT		0.86 ± 0.09

S3 Table. Linear regression R^2 coefficients of the low-frequency PSD fit during quiet standing in the different subjects for both 'x' and 'y' directions.

Subject	*Direction*	*PSD – Linear Regression R^2*	*Subject*	*Direction*	*PSD – Linear Regression R^2*
1	*x*	0.81	14	*x*	0.81
	y	0.81		*y*	0.86
2	*x*	0.67	15	*x*	0.74
	y	0.75		*y*	0.85
3	*x*	0.87	16	*x*	0.30
	y	0.73		*y*	0.67
4	*x*	0.79	17	*x*	0.71
	y	0.73		*y*	0.66
5	*x*	0.70	18	*x*	0.48
	y	0.78		*y*	0.83
6	*x*	0.78	19	*x*	0.72
	y	0.73		*y*	0.77
7	*x*	0.76	20	*x*	0.32
	y	0.83		*y*	0.81
8	*x*	0.46	21	*x*	0.56
	y	0.71		*y*	0.71
9	*x*	0.76	22	*x*	0.76
	y	0.78		*y*	0.82
10	*x*	0.65	23	*x*	0.78
	y	0.67		*y*	0.57
11	*x*	0.64	24	*x*	0.49
	y	0.78		*y*	0.70
12	*x*	0.75	25	*x*	0.72

	y	0.81		*y*	0.83
13	*x*	0.29	26	*x*	0.60
	y	0.77		*y*	0.68
	TOT				0.70±0.14

Linear Regressions of Variance

For each subject in the crank-turning and hand-posture data, the variance trend with respect to time was computed across trials – see the Methods section for details of the computation. For each motor task and for each subject, a linear regression model was fitted to the variance. In the crank-turning task, the linear model was fit over the entire trial duration. Tables S4 and S5 report the R^2 coefficients for each subject respectively in the crank-turning and hand-posture tasks.

S4 Table. Linear regression R^2 coefficients for fits to the variance over time during crank turning in different subjects.

Subject	*Variance – Linear Regression* R^2
1	0.96
2	0.96
3	0.96
4	0.97
5	0.98
6	0.96
7	0.96
8	0.99
9	0.91
10	0.98
TOT	0.96±0.02

S5 Table. Linear regression R^2 coefficients for fits to the variance over time during the hand-posture task in the different subjects for both 'x' and 'y' directions. The table reports the R^2 for both the initial part with linearly growing variance until the breakpoint (t_{bp}) and for the variance over the entire trial duration.

Subject	*Direction*	*Variance – Linear Regression* R^2 ($t \leq t_{bp}$)	t_{bp} $[s]$	*Variance – Linear Regression* R^2 ($\forall\, t$)
1	x	0.92	75.00	0.38
	y	0.95	50.00	0.07
2	x	0.83	4.00	0.00
	y	0.83	5.00	0.00
3	x	0.64	16.00	0.02
	y	0.91	7.00	0.58
4	x	0.95	0.99	0.03
	y	0.97	2.00	0.01
5	x	0.81	136.00	0.30
	y	0.95	38.00	0.35
6	x	0.87	42.00	0.22
	y	0.76	35.00	0.04
7	x	0.90	0.99	0.05
	y	0.88	10.00	0.08
8	x	0.76	19.00	0.00
	y	0.75	44.00	0.00
9	x	0.69	10.00	0.05
	y	0.80	16.00	0.01
10	x	0.93	108.00	0.00
	y	0.95	61.00	0.06
TOT		0.85±0.10		0.11 ± 0.16

In the hand-posture task, two best-fit lines were fit: (i) one for the initial linearly growing variance, until the breakpoint was reached (t_{bp}), and (ii) a second one for the entire trial duration. The breakpoint time $\left(t_{bp}\right)$ was identified as the time presenting the maximum linear fitting performance. This was found by computing the linear regression for increasing time windows and identifying the time window at which R^2 reached a maximum value, after which it declined. The search was performed in increments of $\Delta t = 1\ s$, spanning from a minimum window of $1\ s$ to a maximum window of $200\ s$. Table S5 summarizes the R^2coefficients for both fits and reports the breakpoint time for each subject.

Data Availability

All data are available in the main text or the supplementary information. The MATLAB code and the experimental data are available at the following link https://github.com/jameshermus/brownianProcess/tree/main